Snowcover Identification Using the Special Sensor Microwave Imager

N.C. GRODY[1] AND A.N. BASIST[2]

ABSTRACT

The Special Sensor Microwave Imager (SSM/I) was developed as part of the Defense Meteorological Satellite Program (DMSP) to measure various surface and atmospheric parameters. The instrument was first launched in June 1987 aboard the F-8 polar orbiting satellite and later placed aboard the F-10 and F-11 satellites. A decision tree algorithm was developed to identify snowcover and filter out false signatures due to precipitation, cold deserts and frozen ground surfaces. This paper describes the algorithm developed at NOAA to identify snowcover using SSM/I measurements. Comparisons are made between the SSM/I derived snowcover and the weekly composite product produced operationally by NESDIS using visible satellite imagery.

Key Words: SSM/I, Snowcover

INTRODUCTION

Satellite instruments are particularly useful for measuring the global distribution of snowcover. Snowcover measurements from space began in 1966 with the launch of NOAA's first polar orbiting satellite capable of obtaining visible images of the earth. Since that time, an operational snowcover product has been produced weekly for the northern hemisphere by subjectively analyzing the last clear visible images of the week [Matson et al., 1986]. These drawings of snow extent are digitally scanned, and then archived as a coarse 190 km (89 x 89 grid) resolution map. The entire process takes about 8 to 10 hours each Monday. Besides being highly subjective and manually intensive, data acquisition can be greatly hampered by cloud cover, sometimes at critical times when new snowfall occurs or old snow melts. As such, it does not meet the needs of weather forecast models which require daily measurements (Peterson and Hoke, 1989). The cloud-penetrating property of microwaves overcomes the major limitation associated with visual images. However, as discussed in this paper, microwaves has its own limitations which must be delt with. A global procedure is developed to identify snowcover from daily SSM/I meaurements using objective techniques without manual intervention.

Microwave radiometers aboard satellites have been used to observe the earths surface under cloud covered conditions and identify precipitation (e.g., Ferraro et al, 1986). Unfortunately these measurements were previously only available for research by instruments aboard Nimbus satellites, such as the Scanning Multichannel Microwave Radiometer (SMMR) on Nimbus 7. However, beginning in 1987, the Air Force has launched three Special Sensor Microwave Imager's (SSM/I) into polar orbit aboard the F-8, F-10 and F-11 DMSP satellites. Data from this sensor is routinely processed by the Navy and Air Force as well as by NOAA.

The SSM/I contains dual polarized channels at 19, 37 and 85 GHz and a vertically polarized channel at 22 GHz (Hollinger et al., 1987). These channels are particularly useful for measuring the snowcover and rainfall over land. Over oceans the SSM/I provides

[1]NOAA/NESDIS/ORA/SRL; Washington, D.C. 20233; and [2]NOAA/NWS/NMC/CAC; Washington, D.C. 20233 USA

measurements of rainfall, cloud liquid water, water vapor, sea surface winds and sea ice concentration. Although many of these parameters were obtained using earlier satellite instruments (e.g., SMMR), the SSM/I is the first sensor to contain an 85 GHz channel, which significantly increases the sensitivity and spatial resolution (15 km) to identify precipitation and snowcover. This paper describes the algorithm developed at NOAA to identify snowcover, and contains improvements to the original algorithm (Grody, 1991).

SCATTERING SIGNATURES OVER LAND

Since the launch of the Nimbus-E Microwave Spectrometer (NEMS) on Nimbus-5, it has been recognized that the ice particles within snow are strong scatterers of microwave radiation (Kunzi et al., 1976). More recently, SMMR measurements have shown that large (millimeter size) ice particles produced as part of the precipitation process also scatters microwave radiation (Spencer et al., 1983). Less intense scattering results from the liquid rain drops themselves. In addition to the scattering by ice and water, studies using SSM/I data have shown that sandy deserts and dry bare soils can also scatter microwave radiation (Neale et al., 1990). As discussed later, these sparsely vegetated dry surfaces can be misclassified as snowcover or rain if not accounted for. In order to develop a global algorithm for identifying snowcover it is therefore necessary to understand and account for a wide variety of surfaces as well as precipitation.

Scattering within the media (volume scattering) results in a decreased brightness temperature for increasing frequency. The physical basis of this scattering signature is best illustrated by referring to Figure 1, which shows a simplified diagram of the radiation transfer for both snowcover and precipitation. In both cases, T_u represents the upwelling brightness temperature emitted below the ice-scattering layer and T_b is the radiation emerging from the top of the layer. Ice particles produce little absorption or emission at microwave frequencies so that T_b can be approximated as,

$$T_b(\nu) = \tau_{sc}(\nu)\, T_u$$

where τ_{sc} is the transmittance of the scattering layer at frequency, ν. A more exact model of precipitation would include an emission contribution due to liquid water drops within the ice layer.

The transmittance defines the percent of incident radiation, T_u, that is not scattered by the ice particles. Neglecting multiple scattering, the transmittance of a uniform layer of particles having thickness L is

$$\tau_{sc}(\nu) = \mathrm{Exp}\left[-L \int_0^\infty \pi a^2\, Q_e(a/\lambda)\, n(a)\, da \right]$$

where the integral contains the density of ice particles, n(a), having radius a, and the scattering cross section, $\pi a^2 Q_e$. The frequency dependence of transmittance (and brightness temperature) is defined by the efficiency factor, Q_e, which depends on the ratio of particle radius to radiation wavelength λ. Considering spherical particles, Figure 2 shows a plot of Q_e as a function of particle diameter for the SSM/I frequencies of 19, 37 and 85 GHz. For newly formed snow or light rain the particles are generally less than 2 mm so that Rayleigh scattering applies (i.e., $Q_e \propto \nu^4$) and the cross-section at 85 GHz is about 27 times greater than at 37 GHz. In the case of refrozen snow or convective rain the ice particles are much larger. This results in smaller differences in both Q_e as well as the brightness temperatures of the two channels (see Fig. 2).

Models such as that discussed above provide insight on the physical mechanisms affecting the channel measurements and are in general agreement with actual data. Examples of actual SSM/I measurements are shown in Figure 3 for snowcover, rain and deserts. Both vertical and horizontal polarization measurements are shown, although the largest scattering signature occurs for vertical polarization. The snowcover data is from Canada and the United States during February 1993, while the light and heavy rain were obtained over Texas during November, 1987. Figure 3 also shows the measurements obtained in the cold Gobi desert and hot Sahara desert during February 1993. These sandy deserts display a decrease in the vertical polarized brightness temperature for increasing frequency, which is weaker than the scattering signatures shown for snow and rain. The smallest scattering signatures occur for sparsely vegetated dry soils, which are not shown in the Figure but is discussed later.

The different spectral characteristics illustrated in Figure 3 enable the SSM/I to identify snowcover with minimal ambiguity. As discussed next, a decision tree is used to identify and filter out various features that can lead to misclassification. The

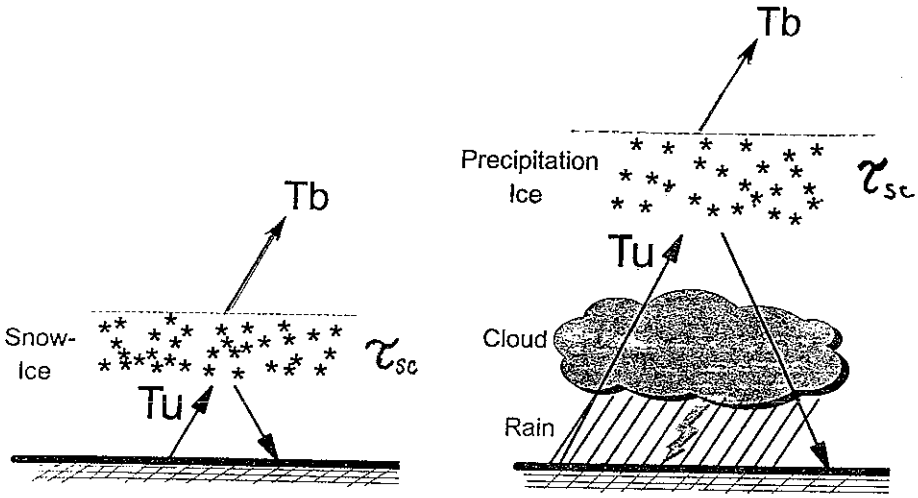

Figure 1. Schematic of different radiation contributions and variables contained in the scattering model for snowcover (left) and precipitation (right). Ice particles within snowcover and precipitation attenuate the upwelling radiation, T_u, through volume scattering.

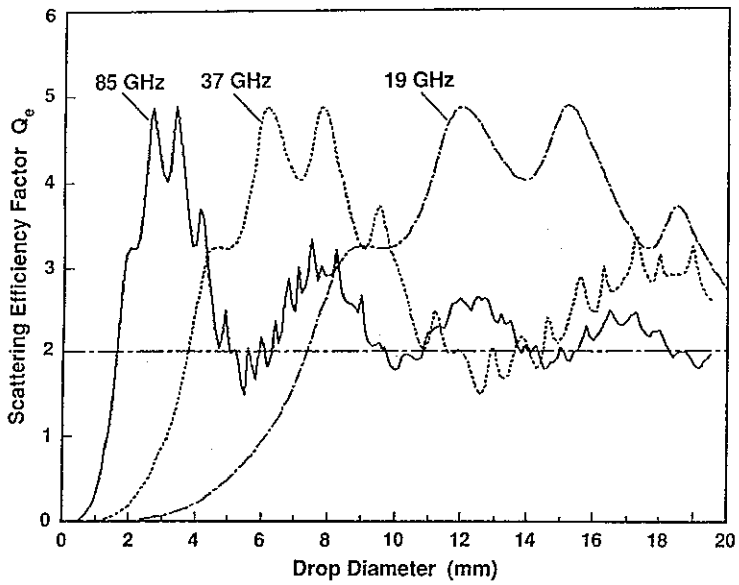

Figure 2. Scattering efficiency for spherical ice particles as a function of diameter.

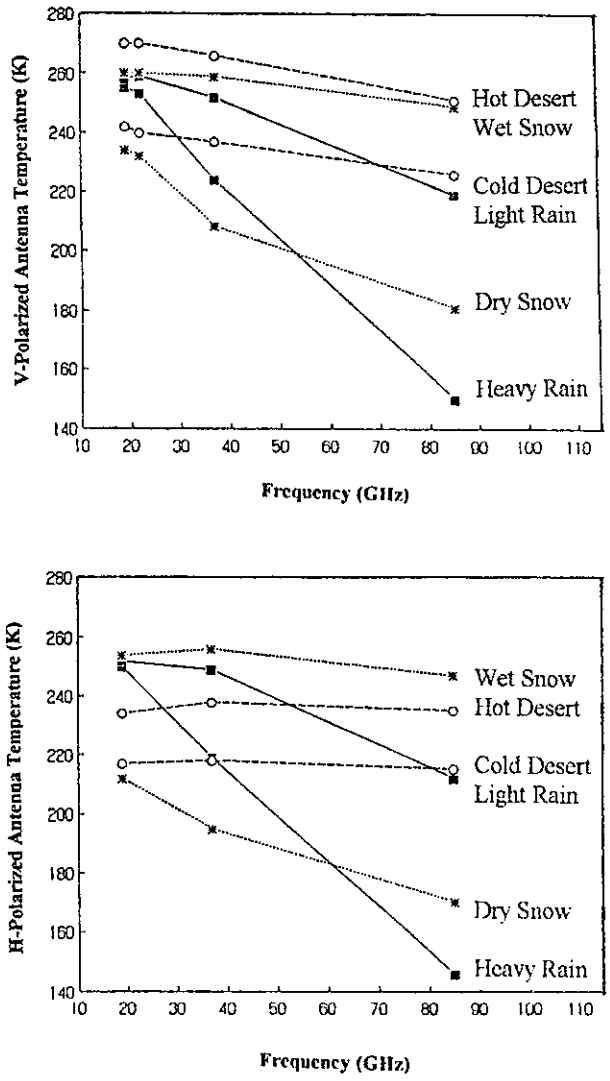

Figure 3. Examples of SSM/I measurements for snowcover, precipitation and deserts. Both vertical (top) and horizontal (bottom) antenna temperatures are shown.

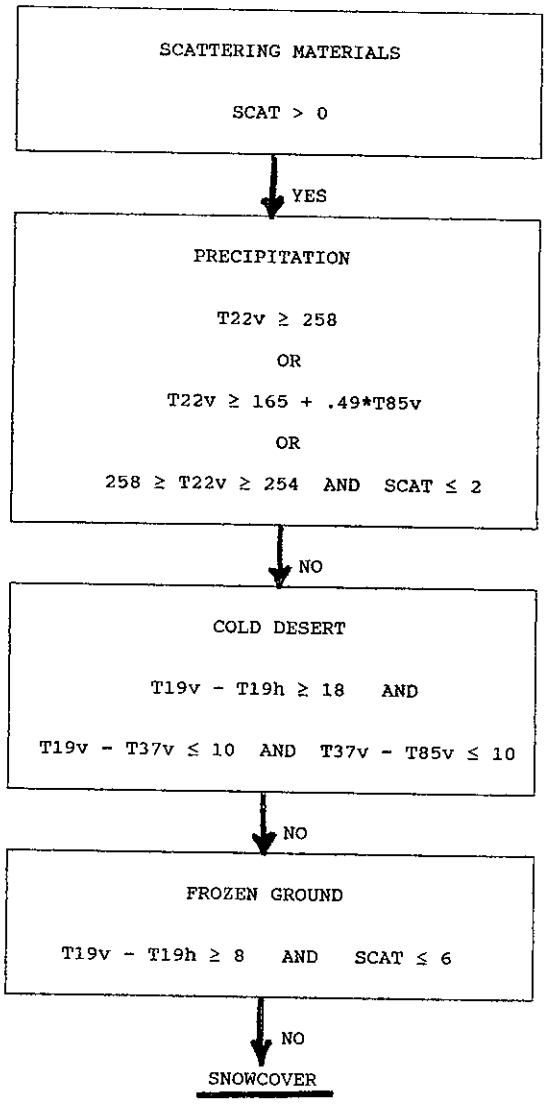

Figure 4. Decision tree to identify snowcover. The filters remove precipitation, cold deserts and frozen ground.

filters are based on the physical knowledge of microwave characteristics as well as empirical observations. Figure 4 shows the decision tree developed for identifying snowcover and is discussed in detail below. It should be noted that the original SSM/I measurements, called antenna temperatures, are used throughout this paper. Brightness temperatures contain a correction to account for the fractional amount of cold-space radiation collected by the antenna when viewing earth. The corrections at 19, 22, 37 and 85 GHz are about 7, 6, 4 and 3 K, and must be added to the antenna temperatures when using brightness temperatures.

SNOWCOVER IDENTIFICATION

As discussed above, snowcover produces a positive difference between the low and high frequency SSM/I channels. Although this scattering signature identifies snow, it also represents precipitation, sandy deserts and cold bare ground. The latter two surfaces were not accounted for earlier (Grody, 1991) but are included in the improved decision trees developed here.

The first step in the identification of snowcover is given by

$$T22v - T85v > 0 \qquad (1a)$$

OR

$$T19v - T37v > 0 \qquad (1b)$$

where T19v, T22v, T37v and T85v denotes the vertically polarized antenna temperatures at the four respective frequencies. In general, (1a) is sufficient to identify snowcover, although (1b) provides an additional check when there is considerable cloud liquid water. The relationships given by (1a) and (1b) are used throughout the paper with different thresholds and shall be denoted as SCAT > N, when N is the threshold. As shown in Figure 4, the constraint SCAT >0 represents the first of many steps.

Precipitation Filter

The density and size of ice particles found in snow are generally larger than those in precipitating systems. Snowcover therefore produces larger scattering effects at low frequencies than precipitation. Furthermore, even in the absence of low frequency scattering, the low frequency measurements are coldest for snowcovered surfaces. Based on these factors, precipitation is identified when the 22 GHz measurements[1] are greater than a given threshold, i.e.,

$$T22v > 257. \qquad (2a)$$

The 257 K threshold represents average conditions and can deviate by ±3 K depending on the surface and atmospheric conditions. For example, melting snow can increase T22v to about 260 K (see Fig. 2) while cold rain can reduce T22v to 254 K. Presently, no global technique has been developed to retain melting snow, although an algorithm based on the 37 GHz polarization difference has been used on a regional basis (Walker and Goodison, 1993). To minimize the problem associated with melting snow only the early morning satellite observations are used. Also, cold rain is approximately filtered using the relationships;

$$T22v \geq 254 \quad AND \quad SCAT \leq 2 \qquad (2b)$$

where these conditions are based on the smaller scattering signatures generally observed for cold rain than for snowcover.

Although (2a) and (2b) are the primary conditions to filter precipitation, a third relationship is needed to account for deep convective rain. Convective rain contains large ice particles (>10 mm) so that scattering occurs at 22 GHz as well as at higher frequencies (see Fig. 3). This reduces T22v below the 257 K threshold, and occurs when T85v is less than about 188 K. As such, the following condition must also be included to filter out precipitation[2] ;

$$T22v \geq 165 + .49\ T85v \qquad (2c)$$

where (2a), (2b) and (2c) define the second step in

[1]The 22 GHz channel was chosen (rather than 19 GHz) since water vapor absorption reduces the channels sensitivity to surface emissivity variations for moist atmospheres. As such, its measurements are generally greater than 257 K, even for light rain over wet surfaces.

[2]In the earlier study (Grody, 1991), the 85 GHz measurements were convolved to the 22 GHz resolution of 55 km, whereas the full resolution (15 km) measurements are used here. The higher resolution results in larger peak scattering values at 85 GHz, which is reflected by the larger intercept in (2c).

the decision tree of Figure 4. As an important side benefit, (2a) also filters out warm deserts, although cold deserts are not removed.

Cold Deserts

The cold deserts found in outer Mongolia, Tibet and central Iran scatter microwave radiation and must be accounted for since T22v is less than the 257 K threshold. These regions contain little vegetation so that they produce a large polarization difference at 19 GHz (see Fig. 3). Unfortunately, snowcover can occasionally produce similar scattering and polarization signatures. After considering various channel combinations, the following set of conditions were found to best filter cold deserts without significantly removing any snowcover;

$$T19v - T19h \geq 18 \quad \text{AND} \qquad (3a)$$

$$T19v - T37v \leq 10 \quad \text{AND} \quad T37v - T85v \leq 10 \qquad (3b)$$

These conditions are used as the third step in the decision tree.

Frozen Ground

In addition to cold deserts, observations of SSM/I data indicate that sparsely vegetated areas of high elevation can produce a small scattering signature during cold periods. Such areas include North Africa, Western Bolivia, New Mexico and the Great Basin of the United States. These dry soils are usually snow-free during their corresponding cold season but produce scattering values between 1 and 6 K due to the thermal gradient within the soil as well as its scattering property (England, 1990). Since these frozen surfaces often occur adjacent to areas having actual snowcover, they can be misinterpreted as light snowcover if not accounted for.

As in the case of cold deserts, a compromising set of conditions is sought to filter frozen ground surfaces without removing any significant amounts of snowcover. Compared to snowcover, frozen ground generally produces a lower scattering signature with a higher polarization difference at 19 GHz, i.e.,

$$SCAT \leq 6 \quad \text{AND} \quad T19v - T19h \geq 8 \qquad (4)$$

where these relationships define the last step of the decision tree in Figure 4.

SUMMARY AND CONCLUSIONS

This paper develops an algorithm in the form of a decision tree to identify the global distribution of snowcover from SSM/I measurements. Since snowcover scatters high frequency radiation, this signature provides the first step of the decision tree shown in Figure 4. Unfortunately, scattering signatures also occur for precipitation, deserts and frozen ground surfaces. Various validation data sets were used to confirm which areas are truly snow covered, and filters were developed to separate snowcover from all other scatterers (see Fig. 4).

The objectively derived snowcover obtained from the SSM/I has great application in an operational mode. This is particularly true for forecast models, which require daily measurements. The monthly produced snow maps are applicable to hydrologic studies pertaining to climate and global change studies. These applications require highly stable sensors, and objectively derived snowcover for detecting small climatic changes.

The SSM/I measurements from the F-10 and F-11 satellites are currently used by NOAA/NESDIS to produce daily snowcover fields on a $1/3^{o}$x$1/3^{o}$ latitude-longitude grid using the decision tree algorithm. The two satellites offer up to four observation a day in some areas. For climate analysis, the daily observations are combined to produce the monthly average snowcover.

During the past year the Climate Analysis Center (CAC) of NOAA has began an extensive evaluation of the SSM/I experimental product by comparing its result with the NESDIS operational snowcover product (see section 1). As an example, Figure 5 shows the comparisons contained in the March Issue of the Climate Diagnostic Bulletin. The Figure displays the percentage of days having snowcover in the northern hemisphere for March, 1994 based on the SSM/I (right) and the operational analysis (left). Percent variations in snowcover is indicated by the gray scale at the bottom of the Figure. Differences between the two results are attributed to the fact that the SSM/I product uses daily observations, while the operational analysis averages four weekly products to obtain the monthly snowcover. Smallest differences between the two analysis are noted where snowcover was observed for the entire month. However, large differences occur where snowcover was less persistent during the month, such as over the northern tier of the United States, southwestern and southeastern Canada, the Alps, Tibet, and many mountain ranges around the hemisphere. Similar results are found for February and April, 1994.

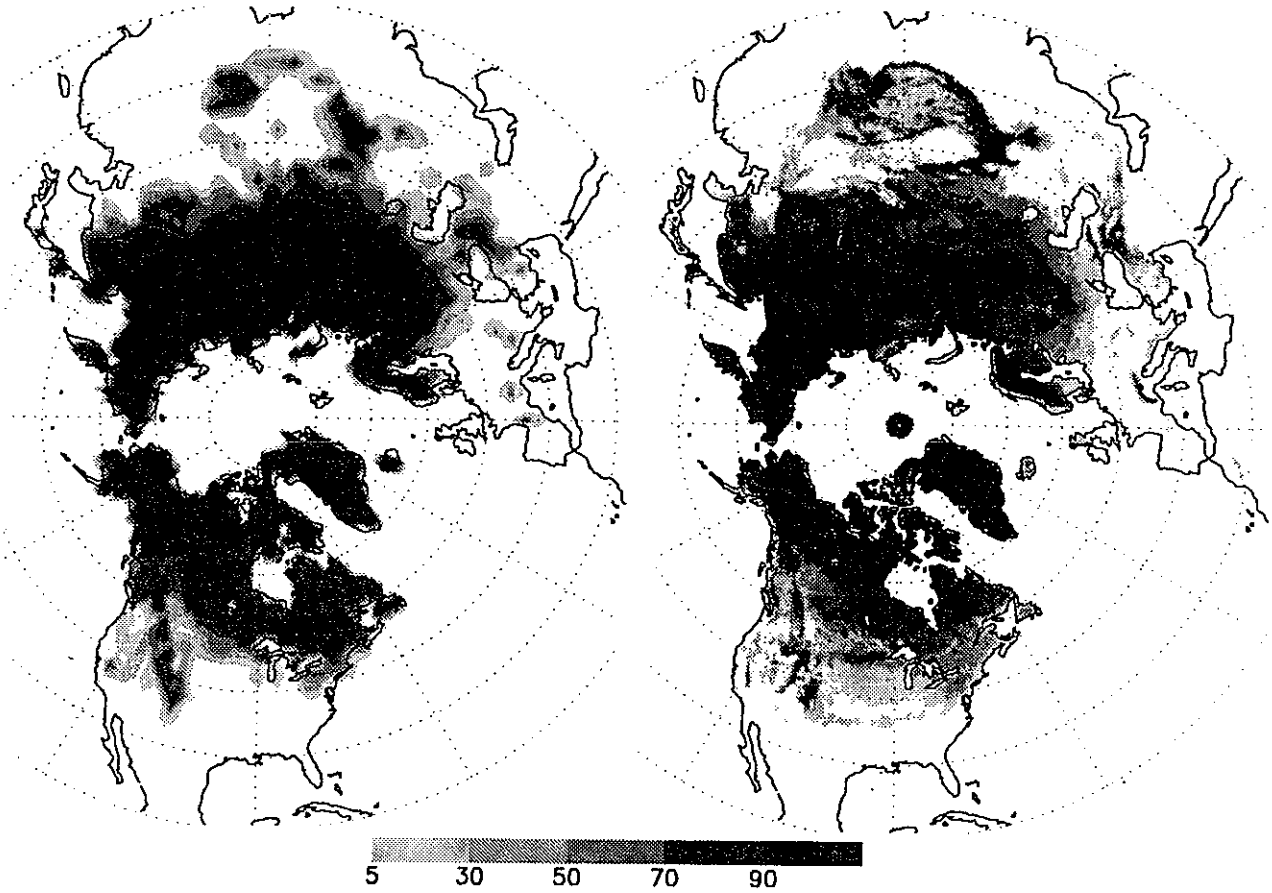

Figure 5. Northern Hemisphere snowcover distribution during March 1994 based on SSM/I (right) and the NESDIS operational analysis (left). The SSM/I technique indicates the percent of days during the month in which snowcover was observed at a given location. In the NESDIS analysis a given area is identified as being snow covered for the month if at least 50% of the once-weekly analyses indicate snowcover in that area.

REFERENCES

England, A.W., "Radiobrightness of Diurnally Heated, Frozen Soil," IEEE Trans. Geos, Sci. Remote Sensing, 28, 464-476, 1990.

Ferraro, R.R, N.C. Grody, and J.A. Kogut, "Classification of geophysical parameters using passive microwave satellite measurements," IEEE Trans. Geosci. Remote Sensing, GE-24, 1008-1013, 1986.

Grody, N.C.,"Classification of snowcover and precipitation using the special sensor microwave imager," J. Geophys. Res., 96, 7423-7435, 1991.

Hollinger, J.R., B. Lo, G. Poe, R. Savage and J. Pierce, "Special Sensor Microwave/ Imager User's Guide," 120 pp., Naval Research Laboratory, Washington, D.C, 1987.

Kunzi, K.F., A.D. Fisher, D.H. Staelin, and J.W. Waters, "Snow and ice surfaces measured by the Nimbus 5 microwave spectrometer," J. Geophys. Res., 881, 4965-4980, 1976.

Matson, M., C.F. Ropelewsky, and M.S. Varnadore, "An atlas of satellite-derived northern hemispheric snow cover frequency," Washington D.C., U.S. Department of Commerce, 1986.

Neale, M.U., M. J. McFarland and Kai Chang, "Land-Surface Classification Using Microwave Brightness Temperatures from the Special Sensor Microwave/Imager," IEEE Trans. Geosci. Remote Sensing, 28, 829-838, 1990.

Peterson, R.A. and J.E. Hoke, "The effect of snow cover on the Regional Analysis and Forecast System (RAFS) low-level forecasts," Wea. and Forecasting, 4, 253-257, 1989.

Spencer, R.W., W.S. Olson, W. Rongzhang, D. Martin, J.A. Weinman and D.A. Santek, "Heavy thunderstorms observed over land by the Nimbus-7 scanning multichannel radiometer," J. Clim. Appl. Meteorol., vol 22, pp. 1041-1046, 1983.

Walker, A.E., and B.E. Goodison, "Discrimination of a wet snowcover using passive microwave satellite data," Annals of Glaciology, vol 17, 1993.